SKY WAVE PROPAGATION AT LOW FREQUENCIES

Radio waves generated by manufactured transmitters near the surface of the earth or radio waves generated by such natural causes as cloud-to-ground lightning strokes propagate to great distances in a lateral direction between the surface of the earth and the ionized region between approximately 60 km and 100 km above the earth. This region is known as the lower ionosphere or the D and E regions of the ionosphere (1–8). These radio waves are called low-frequency (LF) *sky waves* in reference to this propagation phenomenon.

It is common practice to specify 30 kHz to 300 kHz as the LF part of the radio spectrum. This is somewhat arbitrary, and theoretical considerations described herein have been found to be useful far above and below this range of frequencies. In fact, the LF sky wave propagation theory can be used at the lower end of the VLF radio spectrum, and at the higher end of the MF radio spectrum. Traditionally, the mode theory is used at VLF (9), but the theoretical presentations herein can provide an interesting alternative.

Although LF sky waves have been used since the earliest days of radio science, vigorous study of these waves occurred mainly between 1950 and 1970 (see Reading List). This research was in large measure a consequence of the development of precision pulsed ground-wave radio navigation and positioning systems. While the ground wave is very stable with time of day, season, and so on, the ionospheric waves vary with time, and if such waves were not somehow sidestepped, the accuracy and precision of the navigation or positioning system would deteriorate. Thus, from an engineering point of view, LF sky waves were a problem in developing navigation systems such as Loran-C or Loran-D. One direct consequence of this research was the development of the *wave hop theory* of LF sky wave propagation, which will be introduced here. A discussion of Loran-C 100 kHz sky waves is given in Ref. 10.

EXPERIMENTS TO DETECT LOW-FREQUENCY SKY WAVES

An experimental pulse was radiated from a transmitter located in New York state during the 1953 preliminary tests of the Loran-C radio navigation system (2). Figure 1(a,b,c) shows oscillograms of the observed pulse at distances west of the transmitter of 0, 1065, and 1381 km (or 0, 662, 858 statute miles), respectively. The electromagnetic (EM) field near the transmitter is vertically polarized and consists of a pulse that rises to a crest in 4 cycles, or 40 μs. The observation at 1065 km was recorded at 12:55 A.M. EST and therefore includes reflections from the nighttime ionosphere at altitudes as great as 90 km. At 1381 km the second pulse was recorded at 4:00 A.M. EST and the shape reflects the changes that occur between day and night. Finally, the daytime pulse is shown at the distance 1381 km. Here at 9:55 A.M. a daytime sky wave from the D region of the ionosphere dominates the pulse.

It is not difficult to realize that the severe distortion of the pulse is a consequence of multiple reflections from the ionosphere. Thus, many discrete pulses may arrive at the receiver at different delayed points in local times t'. Both the different propagation times and phase distortions resulting from reflection process cause constructive and destructive phase-type interference between the cycles of each pulse.

ELEMENTARY THEORETICAL CONSIDERATIONS

A theory to explain these observed phenomina has been constructed by applying Maxwell's equations to a model of the ionosphere and the earth. Before describing this theory, let

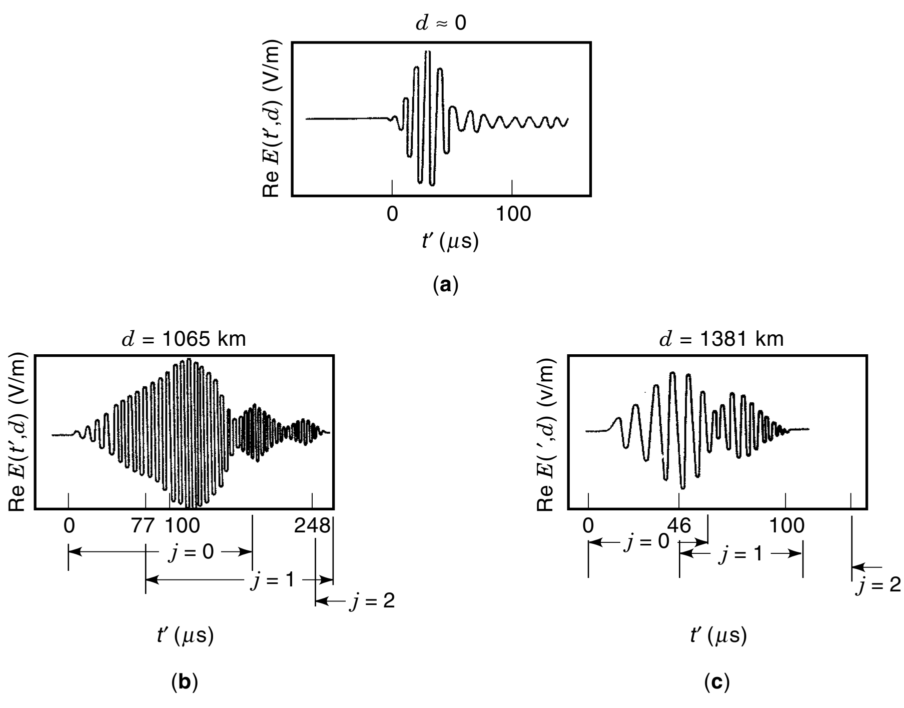

Figure 1. (a) Experimental LF pulse radiation close to the transmitter distance, $d \approx 0$, with a characteristic frequency of 100 kHz. (By permission of IEEE, Ref. 2). (b) Pulse observed at distance d = 1065 km at 12:55 A.M. EST, illustrating nighttime LF sky wave pulses, with characteristic frequency at 100 kHz. (By permission of IEEE, Ref. 2). (c) Pulse observed at a distance of 1381 km at 4:00 A.M. EST, illustrating early morning LF sky wave pulses. (By permission of IEEE, Ref. 2.)

J. Webster (ed.), *Wiley Encyclopedia of Electrical and Electronics Engineering*. Copyright © 1999 John Wiley & Sons, Inc.

us use some simple intuition and a simple model for the propagation environment. Consider the relationship between time and frequency:

$$\boldsymbol{E}(t', d) = \frac{1}{2\pi}\int_{-\infty}^{\infty} \exp(i\omega t)\boldsymbol{E}(\omega, d) f_{\mathrm{s}}(\omega)\, d\omega \qquad (1)$$

where $\boldsymbol{E}(t', d)$ is the propagated field at time t' at a distance d.

Here the transformed field $\boldsymbol{E}(\omega, d)$ depends on the frequency ω, and $t' = t - d/c$, where $c = 0.299792458$ m/ns, a constant. $\boldsymbol{E}(\omega, d)$, and $f_s(\omega)$ are transforms of the field and the source, respectively. The observed pulse is $\boldsymbol{E}(t, d)$, and Re in Fig. 1 denotes the real part (2).

The earliest pulse to arrive at the receiver travels the shortest distance from the transmitter over the geodesic, d. This is the ground wave pulse with the indexed order $j = 0$. Pulses are also reflected from the ionosphere, but these pulses always arrive later in the local time (t') domain. The earliest sky wave to arrive at the receiver at the greater distances occurs during daylight hours. The arrival of the first hop skywave is between 30 μs and 40 μs later than the arrival of the earliest precursor of the ground wave pulse. Thus, the natural world allows only 30 μs to 40 μs of pure ground-wave pulse, in daylight hours, for operation of Loran-C. This difficulty was overcome by time-domain data sampling on the leading edge of the pulse at a point (say less than 30 μs to 40 μs) where pure ground wave pulse energy can be found.

Figure 2 is a diagrammatic representation of the LF sky waves, valid in both the time and frequency domains of Eq. (1) (2,11). The concept of a somewhat localized system of reflection coefficients, R and T, at the ground and at the ionosphere respectively is introduced there. For a spherical model of the earth with a concentric ionosphere as depicted in Fig. 2(a,b), a coordinate system is used such that the distance from the center of the earth to the surface of the ground is $r = a$ and at the ionosphere is $r = a + h$, where r is the radial distance form the center of the earth. The *geodesic distance* is $d = a\theta$, where θ is the angle at the earth's center. The lines connecting the source or transmitter (S) with the observer or receiver (O), via the various local reflecting regions both at the ground and at the ionosphere, are called *geometric-optical rays* (12) or *wave hops* (13), where the latter include diffraction around the curve of the earth. The ionosphere lower boundary is located at $r = a + h = g$. For $r\theta$ coordinates the earth's surface is $r = a$. The earliest part of each sky wave pulse arrives at a time D_j/c, where

$$D_j = 2j[(a + h)\cos\phi_{\mathrm{i},j} - a\cos\tau_j]$$

in which

$\phi_{\mathrm{i},j}$ = angle of incidence on the ionosphere
τ_j = angle of incidence on the earth

If the ionosphere were perfectly conducting (i.e., sharply bounded and of very high conductivity), the reflection coefficient would be $T = -1$. The composite reflection process with

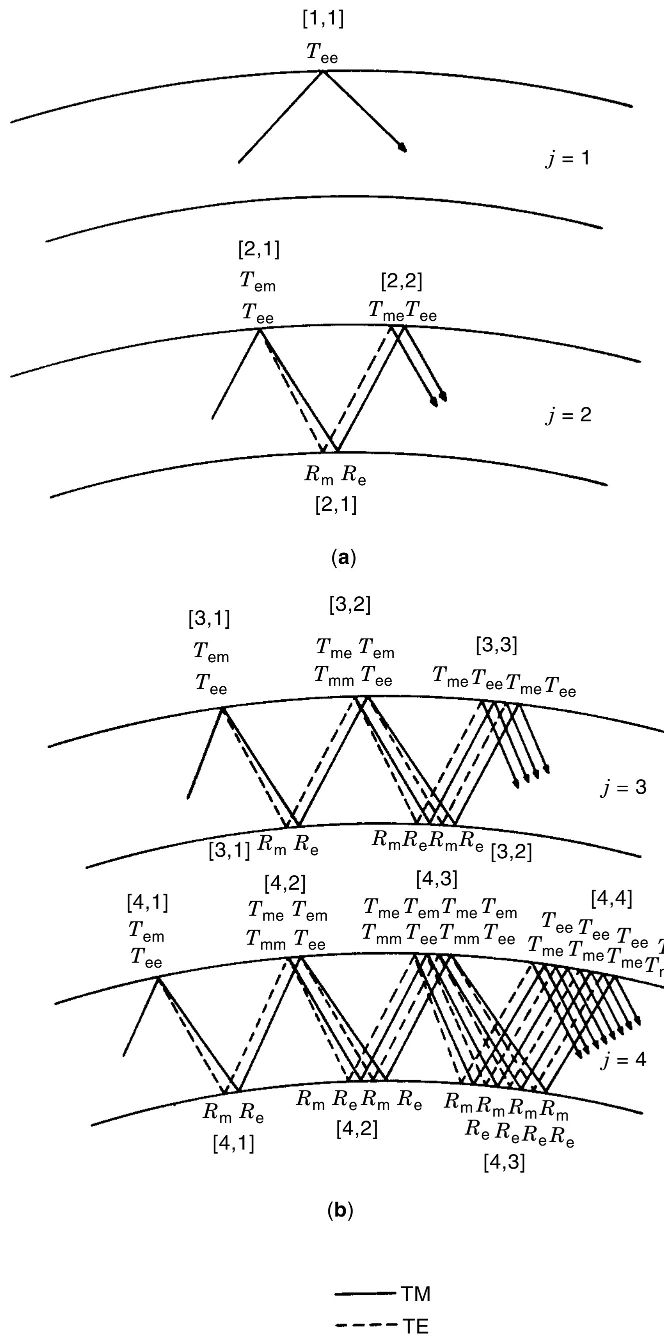

Figure 2. (a) Diagrammatic representation of LF sky waves, depicting an indexing method for identification of a series of time-domain pulses traveling laterally between the ground and the ionosphere, j = 1, 2, 3, ... Reflecting regions at the ionosphere are indicated as (j, k), j = 1, 2, 3, . . ., k = 1, 2, 3, ... (From Ref. 21) (b) Diagrammatic representation of LF sky waves, depicting an indexing method for identification of a series of time-domain pulses traveling laterally between the ground and the ionosphere, j = 2, 4, ... Reflecting regions at the ionosphere are indicated as (j, k), j = 1, 2, 3, . . ., k = 1, 2, 3, ... (From Ref. 21.)

reflections at the ground, R, for any index j would be

$$C_j = (-1)^j p_0^j R_e^{j-1} \tag{2}$$

where

R_e^{j-1} = $(j-1)$th earth reflection coefficient
p_0^j = ionosphere–ground curvature focusing–defocusing factor.

If the ionosphere is simply imperfectly reflecting with a finite conductivity, an ionospheric reflection coefficient T can be introduced:

$$C_j = (T_{ee})^j p_0^j R_e^{j-1} \tag{3}$$

The subscript ee denotes vertical electric (TM, or transverse magnetic) polarization at both the source and the receiver (vertical means in the r direction).

As extensively discussed in the literature (refs. 14–16, for example), the reflection process at the ionosphere is complicated by the effects of the earth's magnetic field on the reflection process. Thus, notwithstanding the fact that the excitation waves generated at the transmitter are pure vertical polarization (TM) waves, such waves arriving at the receiver, after reflecting from the ionosphere magnetoplasma, contain horizontally polarized (TE) wave components. These components of the reflected waves are shown in Fig. 2(a,b) as dashed lines. These dashed geometric-optical lines always originate at the ionosphere magnetoplasma. The ground, for most practical purposes, is considered to be isotropic.

The wave $j = 1$ is independent of the TE waves if the receiving antenna is a vertical structure (i.e., receives only TM waves). But the wave $j = 2$ depends on the TE component, because this component is converted into TM waves at the second reflection point. Thus, in principle, one cannot escape the TE waves that originate in the ionosphere by using vertically polarized transmitting and receiving antennas.

The following reflection coefficients for TM and TE waves are defined as:

T_{ee} is the coefficient for the TM incident, TM reflected wave.

T_{mm} is the coefficient for the TE incident, TE reflected wave.

T_{em} is the TM-incident–TE-reflected conversion coefficient.

T_{me} is the TE-incident–TM-reflected conversion coefficient.

The coupling coefficients for transmission between vertically polarized transmission and reception can now be written:

$$\begin{aligned} C_1 &= T_{ee} \\ C_2 &= R_e T_{ee}^2 + R_m T_{em} T_{me} \\ C_3 &= 2R_e R_m T_{ee} T_{em} T_{me} + R_e^2 T_{ee}^3 + R_m^2 T_{mm} T_{em} T_{me} \\ &\vdots \end{aligned} \tag{4}$$

These equations can be generalized using matrix notation, for vertically polarized transmitters and receivers:

$$G_e = \begin{bmatrix} R_e & 0 \\ 0 & -1 \end{bmatrix} \tag{5}$$

$$T = \begin{bmatrix} T_{ee} & T_{em} \\ T_{me} & T_{mm} \end{bmatrix} \tag{6}$$

$$G_m = p_0 \begin{bmatrix} 1 & 0 \\ 0 & -R_m \end{bmatrix}, \qquad 1 = \begin{bmatrix} 1 & 0 \\ 0 & 1 \end{bmatrix} \tag{7}$$

$$(G_m T G_e)^{j-1} G_m T = p_0^j \begin{bmatrix} C_j & x_j \\ y_j & z_j \end{bmatrix} \tag{8}$$

THEORY OF PROPAGATION OF LOW-FREQUENCY SKY WAVES

Since Eq. (1) is independent of Maxwell's equations, it is necessary only to construct a model for the propagation of the $\boldsymbol{E}$ field in the frequency domain (2,11). The propagation model usually employed to describe the LF sky waves in their natural environment is a finitely conducting spherical earth with radius $r = a$. This spherical earth is surrounded by a *magnetoplasma,* comprising electrons, ions, and neutral particles with a superposed terrestrial magnetic field and a finite frequency of collision between particles. These particles go from random into orbital motion when excited by the LF electromagnetic waves. Each particle has a finite collision frequency, which tends to dampen the activity. Since the earth's magnetic field changes the particle motion from linear to orbital, and the direction of propagation of the EM wave may vary with respect to the terrestrial magnetic field, the ionospheric reflection process becomes anisotropic.

The detailed structure of the lower ionosphere between approximately 60 km and 100 km above the surface of the earth is well documented in the literature (3,17). In the daytime, a layer of such plasma placed at 60 km and concentric with the earth usually serves as a simple model. This can be improved by introducing a large number of such concentric shells of plasma as a function of altitude, to take account of the variation of electron and ion density with altitude. Application of Maxwell's equations to this model results in a rigorous full-wave solution, if the ionosphere is assumed to be isotropic (1). As is indicated in the discussion leading to Eq. (8) and in Refs. 4, 14–16, the curved, concentric, isotropic ionosphere reflection coefficient is normally replaced by a suitable planar anisotropic reflection coefficient. This replacement involves the magneto-ionic theory with a full-wave (plane-wave) reflection coefficient. The spherical-wave focusing effect of the curve ionosphere can be retained in this process.

The LF radio wave field for a transmitter and receiver on the surface of the earth separated by a distance d can be represented rigorously by a system of waves traveling in the radial (r) direction:

$$E_r = A \sum_{n=0}^{\infty} G(\theta, n) F(r, n) \tag{9}$$

Here

$$A = \frac{I_0 L \mu_0 c}{4\pi k_{-1}^2 a^4}$$

where I_0L is the current moment of the source, $\mu_0 = 4\pi \times 10^{-7}$ F/m, $c = 0.299792458$ m/ns, and the wave number for the earth–ionosphere space is $k_{-1} = \omega/c$. We also define

$$k_{-2} = \frac{\omega}{c}\sqrt{\epsilon_{-2} - i\frac{\sigma_{-2}}{\epsilon_0 \omega}}$$

where σ_{-2} is the ground conductivity (s/m), $\omega = 2\pi f$, $\epsilon_0 = 1/c^2\mu_0$, ϵ_{-2} is the relative dielectric constant of the ground, and f the frequency (Hz). Furthermore,

$$G(\theta, n) = n(n+1)(2n+1)P_n(\cos\theta)$$

where $P_0(z) = 1$, $P_1(z) = z$, and

$$P_{n+1}(z) = \frac{2n+1}{n+1} z P_n(z) - \frac{1}{n+1} P_{n-1}(z), \qquad n = 1, 2, \ldots$$

Finally,

$$F(r, n) = \zeta_{-1a}^{(1)} \zeta_{-1a}^{(2)} \frac{(1+R)(1+p_0 T_{\mathrm{ee}})}{1 - p_0 R T_{\mathrm{ee}}} \tag{10}$$

where

$$p_0 = \frac{-\zeta_{-1a}^{(1)}}{\zeta_{-1a}^{(2)}} \frac{-\zeta_{-1g}^{(2)}}{\zeta_{-1g}^{(1)}} \tag{11}$$

$$\begin{aligned} \zeta_{n+1}^{(1,2)}(z) &= \frac{2n+1}{z} \zeta_n^{(1,2)}(z) - \zeta_{n-1}^{(1,2)}(z) \\ \zeta_0^{(1,2)}(z) &= \pm \exp(\mp iz) \\ \zeta_{-1}^{(1,2)}(z) &= \exp(\mp iz) \end{aligned} \tag{12}$$

The abbreviation $\zeta_{-1a}^{(1,2)}$ means $\zeta_{-1}^{(1,2)}(k_{-1}a)$. The earth's reflection coefficient for the spherical waves is

$$R_{\mathrm{e}} = \frac{\ln' \psi_{-1a} - \dfrac{k_{-1}}{k_{-2}} \ln' \psi_{-2a}}{-\ln' \zeta_{-1a}^{(2)} + \dfrac{k_{-1}}{k_{-2}} \ln' \psi_{-2a}}$$

$$\psi_n(z) = \tfrac{1}{2}[\zeta_n^{(1)}(z) + \zeta_n^{(2)}(z)]$$

where $\ln'$ is the logarithmic derivative defined by

$$\ln' \psi_{-1a} = \left[\frac{\psi_n'(z)}{\psi_n(z)}\right]_{z=k_{-1}a}, \qquad \psi_n'(z) = \frac{d}{dz}\psi_n(z)$$

These spherical wave functions are given in Ref. 18.

Equation (10) is derived from this isotropic model by identification of T_{ee} as the reflection coefficient of the lower boundary of this model. If T_{ee} is calculated by the recursion process described in Ref. 1, a rigorous solution of the problem for an arbitrary variation of the electron and ion densities with altitude can be found.

GEOMETRIC SERIES REPRESENTATION

Equation (10) can be expanded into a geometric series:

$$F(r, n) = (1+R)(1+p_0 T_{\mathrm{ee}}) \left(1 + \sum_{j=1}^{\infty} (p_0 R T_{\mathrm{ee}})^j\right) \zeta_{-1a}^{(1)} \zeta_{-1a}^{(2)} \tag{13}$$

for

$$|p_0 R T_{\mathrm{ee}}| < 1 \tag{14}$$

which converges absolutely. The propagated field of Eq. (9) can now be written

$$E_r = E_{r,0} + \sum_{j=1}^{\infty} E_{r,j} \tag{15}$$

where at the surface of the ground the zero-order term is the ground wave:

$$E_{r,0} = B \sum_{n=0}^{\infty} G(\theta, n) \zeta_{-1a}^{(1)} \zeta_{-1a}^{(2)} (1 + R_{\mathrm{e}}) \tag{16}$$

Here

$$B = \frac{\mu_0 c}{8\pi} \frac{I_0 L}{k_{-1}^2 a^4}$$

and R_{e} is the ground reflection coefficient:

$$1 + R_{\mathrm{e}} = \frac{2i}{\zeta_{-1a}^{(1)} \zeta_{-1a}^{(2)} [-\ln' \zeta_{-1a}^{(2)} + (k_{-1}/k_{-2}) \ln' \zeta_{-1a}^{(2)}]}$$

where the logarithmic derivative is

$$\ln' \zeta_{-1a}^{(1,2)} = \left[\frac{\zeta^{(1,2)'}(z)}{\zeta_n^{(1,2)}(z)}\right]_{z=k_{-1}a}$$

with

$$\zeta_n^{(1,2)'}(z) = \frac{d}{dz}\zeta_n^{(1,2)}$$

The quantity B contains I_0L, the source dipole current moment, and $I_0L = 1$ A·m determines the $\boldsymbol{E}$-field amplitude.

A particular sky wave can now be written

$$E_{r,j} = B \sum_{n=0}^{\infty} G(\theta, n) \zeta_{-1a}^{(1)} \zeta_{-1a}^{(2)} (1 + R_{\mathrm{e}})^2 p_0 R_{\mathrm{e}}^{j-1} T_{\mathrm{ee}}^j \tag{17}$$

The anisotropic sky waves can now be written using Eqs. (5)–(8):

$$F(r, n) = (1 + R_{\mathrm{e}}) \frac{|1 + G_{\mathrm{m}} T|}{|1 - G_{\mathrm{m}} G_{\mathrm{e}} T|} \zeta_{-1a}^{(1)} \zeta_{-1a}^{(2)} \tag{18}$$

whereupon expansion of the determinate ratio in a geometric series yields

$$F(r, n) = \zeta_{-1a}^{(1)} \zeta_{-1a}^{(2)} (1 + R_{\mathrm{e}}) \left| \mathbf{I} + (\mathbf{I} + G_{\mathrm{e}}) \sum_{j=1}^{\infty} (G_{\mathrm{m}} G_{\mathrm{e}} T)^{j-1} G_{\mathrm{m}} T \right| \tag{19}$$

with

$$\mathbf{I} = \begin{bmatrix} 1 & 0 \\ 0 & 1 \end{bmatrix}$$

and so

$$E_{r,j} = \sum_{n=0}^{\infty} G(\theta, n)\zeta^{(1)}_{-1a}\zeta^{(2)}_{-1a}(1+R_e)^2 p_0^j C_j \tag{20}$$

Since the ground wave (16) has been removed as a separate entity, the summation of all the j-terms generalized by Eq. (19) is a full-wave solution for the LF sky waves in the presence of an anisotropic ionosphere. The method for inserting anisotropy is discussed in detail in Refs. 1, 13, 19, 20. Reference 21 describes a computer program to calculate this equation directly.

The ratio of the two determinants in Eq. (18) can be written

$$\frac{|\mathbf{I} + G_m T|}{|\mathbf{I} - G_m G_e T|} = \left| \left(\mathbf{I} + \sum_{j=1}^{\infty} G_m G_e T \right)^j (\mathbf{I} + G_m T) \right| \tag{21}$$

which is equivalent to the determinant in Eq. (19). This is analogous to the determinant given by Eq. (7) in Ref. 19.

Equation (21) was central to the development of a widely distributed computer program (22,23) based on the use of the asymptotic computation methods for spherical wave functions of complex, noninteger order n. This approach is based on Ref. 13.

The j-series expansion discussed above is called by its author the *wave hop series.* In this approach Eq. (9) is rewritten in the complex v plane where a suitable contour c is used (24):

$$E_r = \int_c f(v)(1+R_e)\frac{|\mathbf{I} + G_m T|}{|\mathbf{I} - G_m G_e T|}\, dv \tag{22}$$

Here

$$f(v) = -iA\frac{v^3}{\cos v\pi} P_{v-1/2}(-\cos\theta)\zeta^{(1)}_{-1a}\zeta^{(2)}_{-1a} \tag{23}$$

where $P_{v-1/2}(-\cos\theta)$ is the Legendre function of complex order. The function (23) is the complex-order analog to that given in Eq. (9), and we have (12)

$$\zeta^{(1,2)}_{-1a} = \zeta^{(1,2)}_{v-1/2}(k_{-1}a), \qquad \zeta^{(1,2)}_{v-1/2}(z) = \sqrt{\frac{\pi z}{2}} H^{(1,2)}_v(z)$$

where $H^{(1,2)}_v(z)$ is the well-known Hankel function (24).

The spherical reflection coefficients introduced in Fig. 2 and used in Eqs. (16), (17) can now be written

$$R_e = \frac{\zeta^{(1)'}_{-1a} - \dfrac{k_{-1}}{k_{-2}} D_{-2a}\zeta^{(1)}_{-1a}}{-\zeta^{(2)}_{-1a} + \dfrac{k_{-1}}{k_{-2}} D_{-2a}\zeta^{(2)}_{-1a}} \tag{24}$$

where

$$D_{-2a} = \frac{\zeta^{(m)'}_{-2a}}{\zeta^{(m)}_{-2a}} \approx (-1)^m \sqrt{\left(\frac{v}{k_{-2}a}\right)^2 - 1}$$

provided $n = v - \frac{1}{2}$. This is called the Debye approximation; it is used extensively in the literature, for example Refs. 9, 11, 13, 19, 24, and 25. The isotropic reflection from the ionosphere lower boundary located at altitude h above the earth, or $r = g = a + h$, is

$$T = T^s_{ee} = \frac{-\zeta^{(2)}_{1g}}{\zeta^{(2)}_{1g}} T_{ee} \tag{25}$$

$$T^s_{ee} = \frac{\zeta^{(2)}_{1g} - \dfrac{k_{-1}}{k_3} D_{3g}\zeta^{(2)}_{1g}}{-\zeta^{(1)}_{1g} + \dfrac{k_{-1}}{k_3} D_{3g}\zeta^{(1)}_{1g}} \tag{26}$$

where K_3 is an isotropic wave number representing a simple model ionosphere reflector. The angle of incidence on the ionosphere and the earth shown in Fig. 2(a–d) can now be identified:

$$\phi_{i,j} = \sin^{-1}\frac{v}{k_{-1}g}, \qquad \tau_j = \sin^{-1}\frac{v}{k_{-1}a} \tag{27}$$

Using the expansion given in Eq. (21) for an anisotropic ionosphere and integrating each term of the series along a suitable contour in the complex v plane again gives the ground wave analog of Eq. (16) and a series of terms, each of which is a particular sky wave analog of Eq. (17).

The reduction of Eq. (22) is detailed in Refs. 13, 19.

The wave hop series now becomes

$$E_r = \int_c f(v)(1+R_e)\, dv + \sum_{j=1}^{\infty}\int_c f(v)(1+R_e)^2 p_0^j (a_j T_{ee} + c_j T_{me})\, dv \tag{28}$$

$$\begin{bmatrix} a_j & b_j \\ c_j & d_j \end{bmatrix} = G^1_m G_e T \begin{bmatrix} a_{j-1} & b_{j-1} \\ c_{j-1} & d_{j-1} \end{bmatrix} \tag{29}$$

where

$$\begin{aligned} G^1_m &= \frac{G_m}{p_0} \\ a_1 &= 1 \qquad c_1 = 0 \\ a_j &= R_e(T_{ee}a_{j-1} + T_{me}C_{j-1}) \qquad \text{for } j \geq 2 \\ c_j &= R_m(T_{em}a_{j-1} + T_{mm}c_{j-1}) \qquad \text{for } j \geq 2 \end{aligned}$$

Notwithstanding the fact that only TM waves have been excited and only TM waves are received at the receiver, a TE-type ground reflection coefficient is required at the ground as a result of the effects of the earth's magnetic field on the ionosphere. Thus, due to anisotropy, the TE ground reflection coefficient is required, as found explicitly in Refs. 19, 23:

$$R_m = \frac{\zeta^{(1)'}_{-1a} - \dfrac{k_{-2}}{k_{-1}} D_{-2a}\zeta^{(1)}_{-1a}}{-\zeta^{(2)'}_{-1a} + \dfrac{k_{-2}}{k_{-1}} D_{-2a}\zeta^{(2)}_{-1a}} \frac{\zeta^{(2)}_{-1a}}{\zeta^{(1)}_{-1a}} \tag{30}$$

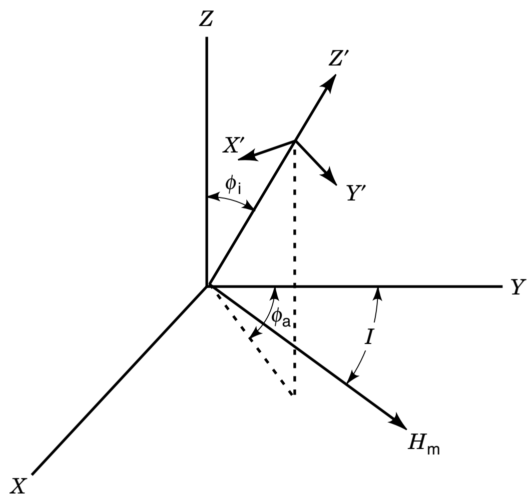

Figure 3. Coordinate system for each reflecting region of the ionosphere.

THEORY OF REFLECTION FROM THE IONOSPHERE

There remains to be explained a reflection process that leads to the four ionosphere reflection coefficients:

$$T_{ee}, \quad T_{mm}, \quad T_{em}, \quad T_{me}$$

The details leading to the mathematical theory of this reflection process are given in Refs. 4, 14, 15, and 16. Consider one of the reflecting regions at the ionosphere depicted in Fig.

Table 1. Coefficients of Quartic Equation for an Electron Plasma

$$a_L = \sin\phi_i \cos\phi_a, \qquad a_T = \sin\phi_i \sin\phi_a$$

$$a_0 = S_2^2\left(1 - \frac{s}{s^2 - h^2}\right) + S_2\left(\frac{1}{s} + \frac{s-2}{s^2-h^2} + \frac{a_T^2 h_T^2}{s(s^2-h^2)}\right) + \frac{s-1}{s(s^2-h^2)}$$

$$a_1 = 2\frac{h_L h_T a_L}{s(s^2-h^2)} S_2$$

$$a_2 = \left[2\left(1 - \frac{s}{s^2-h^2}\right) + \frac{h_L^2}{s(s^2-h^2)}\right] S_2 + \frac{h_L^2 a_T^2}{s(s^2-h^2)} + \frac{s-2}{s(s^2-h^2)}$$

$$a_3 = 2\frac{h_L h_T a_L}{s(s^2-h^2)} - a_L \sec^2\phi_i$$

$$a_4 = 1 - \frac{s^2 - h_L^2}{s(s^2-h^2)}$$

$$s = \frac{\omega^2}{\omega_N^2}\left(1 - i\frac{\nu}{\omega}\right), \qquad S_2 = \sin^2\phi_i - 1$$

$$h = \frac{\omega_H \omega}{\omega_N^2}, \qquad h_L = h\sin I, \qquad h_T = h\cos I$$

$$\omega_N^2 = \frac{Ne^2}{\varepsilon_0 m}$$

$$\omega_H = \frac{\mu_0 e H_m}{m} = \text{gyrofrequency}$$

N and m are the electron number density and mass. H_m is the earth's magnetic intensity; I is the madnetic declination.

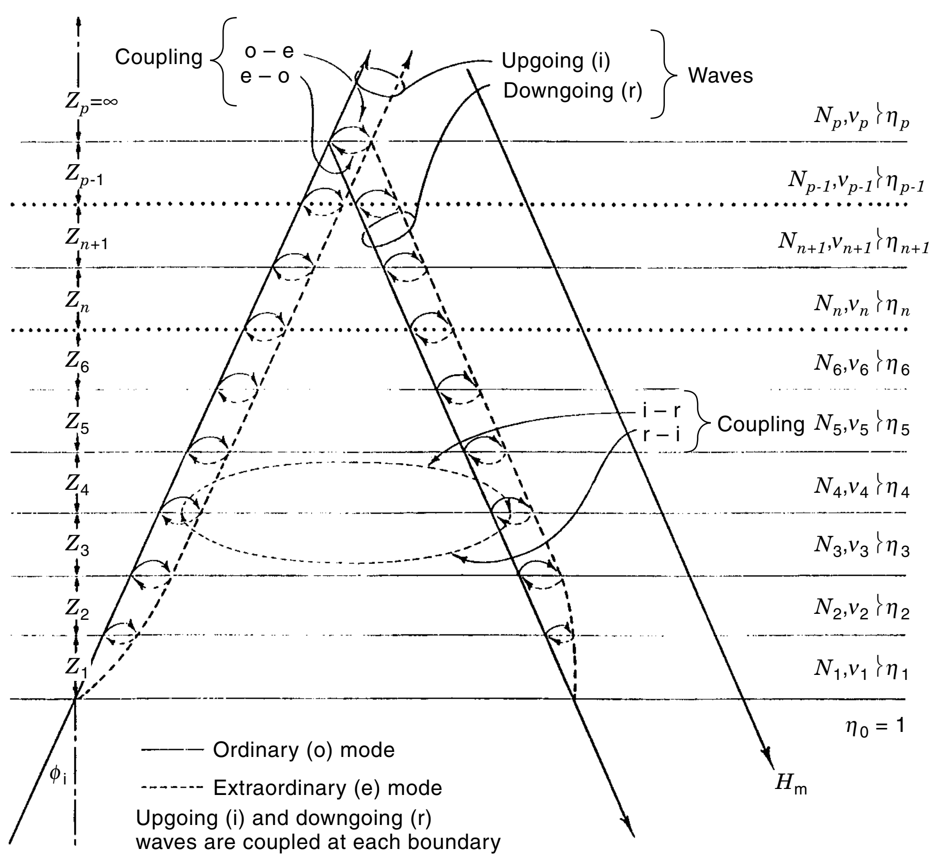

Figure 4. Magnetoplasma model showing detailed structure of the system of waves. The model is flexible, and the number of layers can be increased and the thickness decreased until convergence is obtained on electron–ion density profiles of the lower ionosphere. (After Ref. 2, by permission of IEEE.)

Table 2. Reflection and Transmission Coefficient Matrices

$$
\begin{bmatrix}
a_{11}a_{12}a_{13}a_{14}a_{15}a_{16} & & & & \\
b_{11}b_{12}b_{13}b_{14}b_{15}b_{16} & & & & \\
c_{11}c_{12}c_{13}a_{14}c_{15}c_{16} & & & & \\
d_{11}d_{12}d_{13}d_{14}d_{15}d_{16} & & & & \\
 & a_{23}a_{24}a_{25}a_{26}a_{27}a_{28}a_{29}a_{2(10)} & & & \\
 & b_{23}b_{24}b_{25}b_{26}b_{27}b_{28}b_{29}b_{2(10)} & & & \\
 & c_{23}c_{24}c_{25}c_{26}c_{27}c_{28}c_{29}c_{2(10)} & & & \\
 & d_{23}d_{24}d_{25}d_{26}d_{27}d_{28}d_{29}b_{2(10)} & & & \\
 & & a_{37}a_{38}a_{39}a_{3(10)}a_{3(11)}a_{3(12)}a_{3(13)}a_{3(14)} & & \\
 & & b_{37}b_{38}b_{39}b_{3(10)}b_{3(11)}b_{3(12)}b_{3(13)}b_{3(14)} & & \\
 & & c_{37}c_{38}c_{39}c_{3(10)}c_{3(11)}c_{3(12)}c_{3(13)}c_{3(14)} & & \\
 & & d_{37}d_{38}d_{39}d_{3(10)}d_{3(11)}d_{3(12)}d_{3(13)}d_{3(14)} & & \\
 & & & \cdot\ \cdot\ \cdot\ \cdot\ \cdot\ \cdot\ \cdot\ \cdot\ \cdot\ \cdot\ \cdot & \\
 & & & \cdot\ \cdot\ \cdot\ \cdot\ \cdot\ \cdot\ \cdot\ \cdot\ \cdot\ \cdot\ \cdot & \\
 & & & \cdot\ \cdot\ \cdot\ \cdot\ \cdot\ \cdot\ \cdot\ \cdot\ \cdot\ \cdot\ \cdot & \\
 & & & \cdot\ \cdot\ \cdot\ \cdot\ \cdot\ \cdot\ \cdot\ \cdot\ \cdot\ \cdot\ \cdot & \\
 & & & & a_{p(p+4)}\cdots a_{p(p+9)} \\
 & & & & b_{p(p+4)}\cdots b_{p(p+9)} \\
 & & & & c_{p(p+4)}\cdots c_{p(p+9)} \\
 & & & & d_{p(p+4)}\cdots d_{p(p+9)}
\end{bmatrix}
\begin{bmatrix}
T_{\mathrm{em}} & T_{\mathrm{mm}} \\
T_{\mathrm{ee}} & T_{\mathrm{me}} \\
U^{(1)}_{\mathrm{eio}} & U^{(1)}_{\mathrm{mio}} \\
U^{(1)}_{\mathrm{eic}} & U^{(1)}_{\mathrm{mie}} \\
U^{(1)}_{\mathrm{ero}} & U^{(1)}_{\mathrm{mro}} \\
U^{(1)}_{\mathrm{ere}} & U^{(1)}_{\mathrm{mre}} \\
U^{(2)}_{\mathrm{eio}} & U^{(2)}_{\mathrm{mio}} \\
U^{(2)}_{\mathrm{eie}} & U^{(2)}_{\mathrm{mie}} \\
U^{(2)}_{\mathrm{ero}} & U^{(2)}_{\mathrm{mro}} \\
U^{(2)}_{\mathrm{ere}} & U^{(2)}_{\mathrm{mre}} \\
\cdot & \cdot \\
\cdot & \cdot \\
\cdot & \cdot \\
\cdot & \cdot \\
U^{(p-1)}_{\mathrm{eio}} & U^{(p-1)}_{\mathrm{mio}} \\
U^{(p-1)}_{\mathrm{eie}} & U^{(p-1)}_{\mathrm{mie}} \\
U^{(p-1)}_{\mathrm{ero}} & U^{(p-1)}_{\mathrm{mro}} \\
U^{(p-1)}_{\mathrm{ere}} & U^{(p-1)}_{\mathrm{mre}} \\
U^{(p)}_{\mathrm{eio}} & U^{(p)}_{\mathrm{mio}} \\
U^{(p)}_{\mathrm{eie}} & U^{(p)}_{\mathrm{mie}}
\end{bmatrix}
+
\begin{bmatrix}
a_{\mathrm{oe}} & a_{\mathrm{om}} \\
b_{\mathrm{oe}} & b_{\mathrm{om}} \\
c_{\mathrm{oe}} & c_{\mathrm{om}} \\
d_{\mathrm{oe}} & d_{\mathrm{om}} \\
 & \\
 & \\
 & \\
 & \\
 & \\
 & \\
 & \\
 & \\
 & \\
 & \\
 & \\
 & \\
 & \\
 & \\
 & \\
 &
\end{bmatrix}
= 0
$$

(2a,b). The reflection process at one such region will now be given in detail.

The particle statistics of the electron–ion–neutral gas with superposed electrodynamic and magnetostatic fields was first treated in radio science between 1927 and 1931 (5–8). See also Ref. 26, pp. 59–99.

The use of the full magneto-ionic theory to model LF sky wave propagation is given in Ref. 14. A local coordinate system is set up at a particular reflecting region depicted in Fig. 2. This Cartesian *xyz*, coordinate system is shown in Fig. 3. The terrestrial magnetic field vector is contained in the *yz* plane. The EM wave propagates in the z' direction, and the

Table 3. Elements of Matrix Equation

$a_{11} = \cos\phi_{\mathrm{i}}$	$b_{11} = -\sin\phi_{\mathrm{i}}$
$a_{12} = -\cos\phi_{\mathrm{i}}\sin\phi_{\mathrm{a}}$	$b_{12} = -\cos\phi_{\mathrm{i}}\cos\phi_{\mathrm{a}}$
$a_{13} = -Q^{(1)}_{1\mathrm{o}}$	$b_{13} = -1$
$a_{14} = -Q^{(1)}_{\mathrm{ie}}$	$b_{14} = -1$
$a_{15} = -Q^{(1)}_{\mathrm{ro}}$	$b_{15} = -1$
$a_{16} = -Q^{(1)}_{\mathrm{ro}}$	$b_{16} = -1$
$a_{23} = -a_{13}\exp\left(-i\dfrac{\omega}{c}z_1\,\xi^{(1)}_{\mathrm{io}}\right)$	$b_{23} = \exp\left(-1\dfrac{\omega}{c}z_1\,\xi^{(1)}_{\mathrm{io}}\right)$
$a_{24} = -a_{14}\exp\left(-i\dfrac{\omega}{c}z_1\,\xi^{(1)}_{\mathrm{ie}}\right)$	$b_{24} = \exp\left(-i\dfrac{\omega}{c}z_1\,\xi^{(1)}_{\mathrm{ie}}\right)$
$a_{25} = -a_{15}\exp\left(-i\dfrac{\omega}{c}z_1\,\xi^{(1)}_{\mathrm{ro}}\right)$	$b_{25} = \exp\left(-i\dfrac{\omega}{c}z_1\,\xi^{(1)}_{\mathrm{ro}}\right)$
$a_{26} = -a_{16}\exp\left(-i\dfrac{\omega}{c}z_1\,\xi^{(1)}_{\mathrm{re}}\right)$	$b_{26} = \exp\left(-i\dfrac{\omega}{c}z_1\,\xi^{(1)}_{\mathrm{re}}\right)$
$a_{27} = -Q^{(2)}_{\mathrm{io}}$	$b_{27} = -1$
$a_{28} = -Q^{(2)}_{\mathrm{ie}}$	$b_{28} = -1$
$a_{29} = -Q^{(2)}_{\mathrm{ro}}$	$b_{29} = -1$
$a_{37} = -a_{27}\exp\left(-i\dfrac{\omega}{c}z_2\,\xi^{(2)}_{\mathrm{io}}\right)$	$b_{37} = \exp\left(-i\dfrac{\omega}{c}z_2\,\xi^{(2)}_{\mathrm{io}}\right)$
$\vdots$	$\vdots$
$a_{p(p+9)} = -Q_{1\mathrm{e}}$	$b_{p(p+9)} = -1$

Table 4. Elements of Matrix Equation

$c_{11} = -\cos\phi_{\mathrm{i}}\sin\phi_{\mathrm{a}}$	$d_{11} = -\cos\phi_{\mathrm{i}}\cos\phi_{\mathrm{a}}$
$c_{12} = -\cos\phi_{\mathrm{a}}$	$d_{12} = \sin\phi_{\mathrm{a}}$
$c_{13} = -(a_{\mathrm{L}}P^{(1)}_{\mathrm{io}} - \xi^{(1)}_{\mathrm{io}})$	$d_{13} = -(\xi^{(1)}_{\mathrm{io}}Q^{(1)}_{\mathrm{io}} - a_{\mathrm{T}}P^{(1)}_{\mathrm{io}})$
$c_{14} = -(a_{\mathrm{L}}P^{(1)}_{\mathrm{ie}} - \xi^{(1)}_{\mathrm{ie}})$	$d_{14} = -(\xi^{(1)}_{\mathrm{ie}}Q^{(1)}_{\mathrm{ie}} - a_{\mathrm{T}}P^{(1)}_{\mathrm{ie}})$
$c_{15} = -(a_{\mathrm{L}}P^{(1)}_{\mathrm{ro}} - \xi^{(1)}_{\mathrm{ro}})$	$d_{15} = -(\xi^{(1)}_{\mathrm{ro}}Q^{(1)}_{\mathrm{ro}} - a_{\mathrm{T}}P^{(1)}_{\mathrm{ro}})$
$c_{16} = -(a_{\mathrm{L}}P^{(1)}_{\mathrm{re}} - \xi^{(1)}_{\mathrm{re}})$	$d_{16} = -(\xi^{(1)}_{\mathrm{re}}Q^{(1)}_{\mathrm{re}} - a_{\mathrm{T}}P^{(1)}_{\mathrm{re}})$
$c_{23} = -c_{13}\exp\left(-i\dfrac{\omega}{c}z_1\,\xi^{(1)}_{\mathrm{io}}\right)$	$d_{23} = -d_{13}\exp\left(-i\dfrac{\omega}{c}z_1\,\xi^{(1)}_{\mathrm{io}}\right)$
$c_{24} = -c_{14}\exp\left(-i\dfrac{\omega}{c}z_1\,\xi^{(1)}_{\mathrm{ie}}\right)$	$d_{24} = -d_{14}\exp\left(-i\dfrac{\omega}{c}z_1\,\xi^{(1)}_{\mathrm{ie}}\right)$
$c_{25} = -c_{15}\exp\left(-i\dfrac{\omega}{c}z_1\,\xi^{(1)}_{\mathrm{ro}}\right)$	$d_{25} = -d_{15}\exp\left(-i\dfrac{\omega}{c}z_1\,\xi^{(1)}_{\mathrm{ro}}\right)$
$c_{26} = -c_{16}\exp\left(-i\dfrac{\omega}{c}z_1\,\xi^{(1)}_{\mathrm{re}}\right)$	$d_{26} = -d_{16}\exp\left(-i\dfrac{\omega}{c}z_1\,\xi^{(1)}_{\mathrm{re}}\right)$
$c_{27} = -(a_{\mathrm{L}}P^{2}_{\mathrm{io}} - \xi^{(2)}_{\mathrm{io}})$	$d_{27} = -(\xi^{(2)}_{\mathrm{io}}\,Q^{(2)}_{\mathrm{io}} - a_{\mathrm{T}}P^{(2)}_{\mathrm{io}})$
$c_{28} = -(a_{\mathrm{L}}P^{(2)}_{\mathrm{ie}} - \xi^{(2)}_{\mathrm{ie}})$	$d_{28} = -(\xi^{(2)}_{\mathrm{ie}}Q^{(2)}_{\mathrm{ie}} - a_{\mathrm{T}}P^{(2)}_{\mathrm{ie}})$
$c_{29} = -(a_{\mathrm{L}}P^{(2)}_{\mathrm{ro}} - \xi^{(2)}_{\mathrm{ro}})$	$d_{29} = -(\xi^{(2)}_{\mathrm{ro}}Q^{(2)}_{\mathrm{ro}} - a_{\mathrm{T}}P^{(2)}_{\mathrm{ro}})$
$c_{2\,10} = -(a_{\mathrm{L}}P^{(2)}_{\mathrm{re}} - \xi^{(2)}_{\mathrm{re}})$	$d_{2\,10} = -(\xi^{(2)}_{\mathrm{ie}}Q^{(2)}_{\mathrm{ie}} - a_{\mathrm{T}}P^{(2)}_{\mathrm{re}})$
$c_{37} = -c_{27}\exp\left(-i\dfrac{\omega}{c}z_2\,\xi^{(2)}_{\mathrm{io}}\right)$	$d_{37} = -d_{27}\exp\left(-i\dfrac{\omega}{c}z_2\,\xi^{(2)}_{\mathrm{io}}\right)$
$\vdots$	$\vdots$
$c_{p(p+9)} = -(a_{\mathrm{L}}P^{(p)}_{\mathrm{ie}} - \xi^{(p)}_{\mathrm{ie}})$	$d_{p(p+9)} = -(\xi^{(p)}_{\mathrm{ie}}\,Q^{(p)}_{\mathrm{ie}} - a_{\mathrm{T}}P^{(p)}_{\mathrm{ie}})$

Table 5. Elements of Matrix Equation

$a_{oe} = \cos\phi_i \sin\phi_a$	$a_{om} = \cos\phi_a$
$b_{oe} = \cos\phi_i \sin\phi_a$	$b_{om} = -\sin\phi_a$
$c_{oe} = -\cos\phi_a$	$c_{om} = \cos\phi_i \sin\phi_a$
$d_{oe} = \sin\phi_a$	$d_{om} = \cos\phi_i \cos\phi_a$
$A_1 = -\left(a_L\xi + \dfrac{h_T h_L}{s(s^2-h^2)}\right)\left(1 - a_L^2 - \xi^2 - \dfrac{s}{s^2-h^2}\right)$	
$B_1 = (a_L a_T - i\dfrac{h_L}{s^2-h^2}\Big)\left(a_T\xi - i\dfrac{h_T}{s^2-h^2}\right)$	
$C_1 = -\left(1 - a_s^2 - \dfrac{s^2-h_L^2}{s(s^2-h^2)}\right)\left(a_L a_T - \mathrm{i}\dfrac{h_L}{s^2-h^2}\right)$	
$D_1 = \left(a_T\xi + i\dfrac{h_T}{s^2-h^2}\right)\left(a_L\xi + \dfrac{h_L h_T}{s(s^2-h^2)}\right)$	
$E_1 = \left(1 - a_s^2 - \dfrac{s^2-h_L^2}{s(s^2-h^2)}\right)\left(1 - a_L^2 - \xi^2 - \dfrac{s}{s^2-h^2}\right)$	
$F_1 = -\left(a_T\xi + i\dfrac{h_T}{s^2-h^2}\right)\left(a_T\xi - i\dfrac{h_T}{s^2-h^2}\right)$	
$P = \dfrac{A_1 + B_1}{E_1 + F_1}$	$Q = \dfrac{C_1 + D_1}{E_1 + F_1}$

Here $\xi = \xi^{(n)}$, $P = P^{(n)}$, $Q = Q^{(n)}$ for a particular slab (Fig. 4), and $a_s = \sin\phi_i$; io, ie, ro, re refer to the four roots of Eq. (35).

wavefronts are contained in the $x'y'$ plane. The directions relative to the magnetic field vector are as follows:

ϕ_i is the angle of incidence.
ϕ_a is the magnetic azimuth.
I is the magnetic dip angle.
$\phi_{i,j}$ is now abbreviated to ϕ_i.

Figure 4 depicts a flexible model for the lower ionosphere. The plasma electron density is divided into layers. The thickness of each layer is decreased and the number of layers is increased until a stable reflection coefficient set is obtained for a particular electron number density, collision frequency, and so on. Figure 4 depicts ordinary and extraordinary propagation components coupled at each boundary. Each plasma slab, $n = 1, 2, 3, \ldots, p$, becomes smaller as the number of slabs, p, is increased. The complex index of refraction for each layer in the model is obtained from a simultaneous solution of Maxwell's equations and the equation of motion in the velocity $\boldsymbol{V}$:

$$\nabla \times \boldsymbol{E} + \mu_0 \frac{\partial \boldsymbol{H}}{\partial t} = 0$$
$$\nabla \times \boldsymbol{H} - \boldsymbol{J} - \epsilon_0 \frac{\partial \boldsymbol{E}}{\partial t} = 0 \quad (31)$$

$$m\frac{d\boldsymbol{V}}{dt} + m\nu\boldsymbol{V} + \mu_0 e\boldsymbol{V} \times \boldsymbol{H} + e\boldsymbol{E} = 0 \quad (32)$$

where $\mu_0 = 4\pi \times 10^{-7}$ H/m, ν is the collision frequency, m is the electronic mass, and e is the electronic charge. Reference 4 extends these equations to include ions, and Ref. 16 provides an extension for collision rate proportional to energy (27–29). The lower boundary of the model electron plasma (Fig. 3), below which ($z < 0$) the ionization is nil ($N = 0$), is taken as the xy plane. The region above the xy plane ($z > 0$) is characterized by an electron number density N, which, along with the collision frequency, varies with altitude z. A plane wave incident upon the ionosphere is assumed to be

$$E_i = |\boldsymbol{E}_i| \exp\left[i\left(\omega t - \frac{\omega}{c}\eta D\right)\right] \quad (33)$$

Below the ionosphere, $\eta = \eta_0 = 1$. Here

$$D = x\sin\phi_i \sin\phi_a + y\sin\phi_i \cos\phi_a + z\cos\phi_i$$

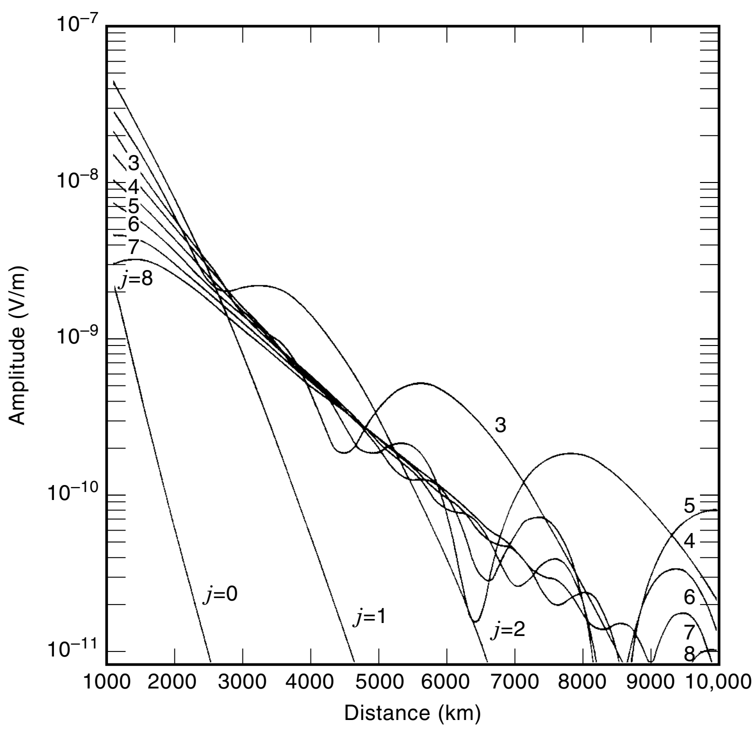

Figure 5. Amplitude of the total $\boldsymbol{E}$ field as a function of distance along the surface of the earth, together with the individual wave hops, $j = 0$ (the ground wave), 1, 2, 3, . . ., illustrating propagation in the presence of an ionosphere with infinite conductivity. (From Ref. 21 by permission IEEE (2).)

A wave transmitted into the ionosphere is assumed to have the form

$$E_t = |\boldsymbol{E}_t| \exp\left[i\left(\omega t - \frac{\omega}{c}\eta D\right)\right] \quad (34)$$

Elimination of the vectors $\boldsymbol{V}$ and $\boldsymbol{H}$ results in a quartic equation:

$$\eta D = x \sin\phi_i \sin\phi_a + y \sin\phi_i \cos\phi_a + z\xi$$
$$a_4\xi^4 + a_3\xi^3 + a_2\xi^2 + a_1\xi + a_0 = 0 \quad (35)$$

The detailed explicit expressions for the coefficients of this quartic are given in Table 1 for an electron magnetoplasma. The coefficients for an electron–ion magnetoplasma are given in Ref. 4. The quartic equation is readily solved numerically with various computer programs that exist in the literature, such as Refs. 21, 22. The complex index of refraction of a particular layer in the model now can be found:

$$\eta^2 = \xi^2 + \sin^2\phi_i \quad (36)$$

The significance of the four roots of the quartic equation is depicted in Fig. 4. There are two upgoing waves, called the ordinary and the extraordinary upgoing wave. There are two downgoing waves, the ordinary and the extraordinary downgoing wave. These four waves are coupled at each boundary in the model and hence are modified by the change in electron density on each side of the boundary.

The boundary of each stratum, or plasma slab, is introduced through the continuity of the tangential $\boldsymbol{E}$ and $\boldsymbol{H}$ field components in Maxwell's equations. This is accomplished by equating the fields immediately above and immediately below each boundary, which results in the matrix equation in Table 2.

Using Fig. 3, the following transmission and reflection coefficients can be recovered by a numerical solution of the matrix equation in Table 2:

$$T_{ee} = \frac{E_{y'r}}{E_{y'i}}, \qquad T_{em} = \frac{E_{x'r}}{E_{y'_i}}$$
$$T_{me} = \frac{E_{y'r}}{E_{x'i}}, \qquad T_{mm} = \frac{E_{x'r}}{E_{x'i}}$$
$$U(n)_{eio} = \frac{E^{(n)}_{yio}}{E_{y'i}}, \qquad U(n)_{mio} = \frac{E^{(n)}_{yio}}{E_{x'i}}$$
$$U(n)_{eie} = \frac{E^{(n)}_{yie}}{E_{y'i}}, \qquad U(n)_{mie} = \frac{E^{(n)}_{yie}}{E_{x'r}}$$

using the ratios $Q = E_x/E_y$, $P = E_z/E_y$, where (Fig. 2) $n = 1, 2, 3, \ldots, p-1$. The elements of the matrix equation in Table 2 are defined in Tables 3, 4, and 5 for an electron magnetoplasma.

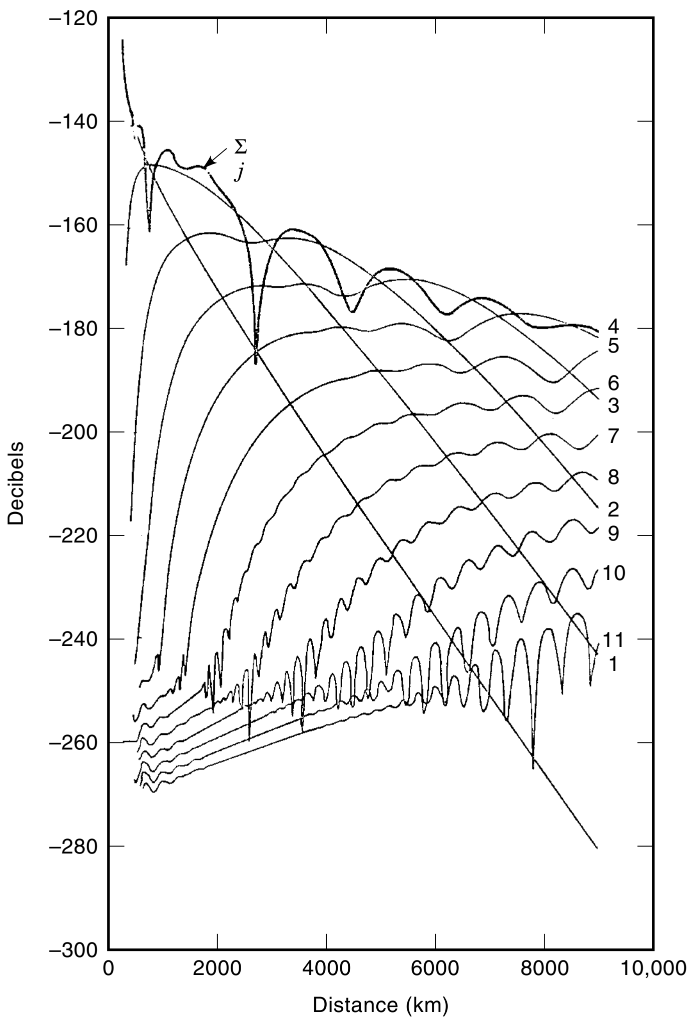

Figure 6. Amplitude of the total $\boldsymbol{E}$ field as a function of distance along the surface of the earth, together with the individual wave hops, $j = 0$ (the ground wave), 1, 2, 3, . . ., illustrating propagation in the presence of a sharply bounded semiinfinite plasma slab placed at the height $h = 65$ km for a signal at 26.1 kHz and an assumed ratio of electron number density to collision frequency equal to 9.375 (1). (From Ref. 1, by permission of AGU.)

SKY WAVE DIFFRACTION

The angle of incidence of the sky wave on the earth [Eq. (26)] is in general complex:

$$\tau_j = \frac{v}{k_{-1}a}$$

This is implied in the full-wave solutions given by Eqs. (16), (17), (26). LF sky wave diffraction theory has been treated in Refs. 25, 30, and 31. However, it can now be demonstrated that the full-wave solution discussed herein implies sky wave diffraction into the earth's shadow region. The hypothetical ionosphere reflection was set equal to that of a perfect reflector [Eq. (2)], and Eqs. (16), (17) were used to generate the wave hop series shown in Fig. 5. Each wave hop in Fig. 5—$j = 0$ (the ground wave) and $j = 1, 2, 3, \ldots$—will ultimately go beyond the geometric-optical horizon, and the attenuation finally takes on a slope as a function of distance like the ground wave. The conductivity of the ground is assumed to be 0.005 S/m with a dielectric constant of 15 relative to space.

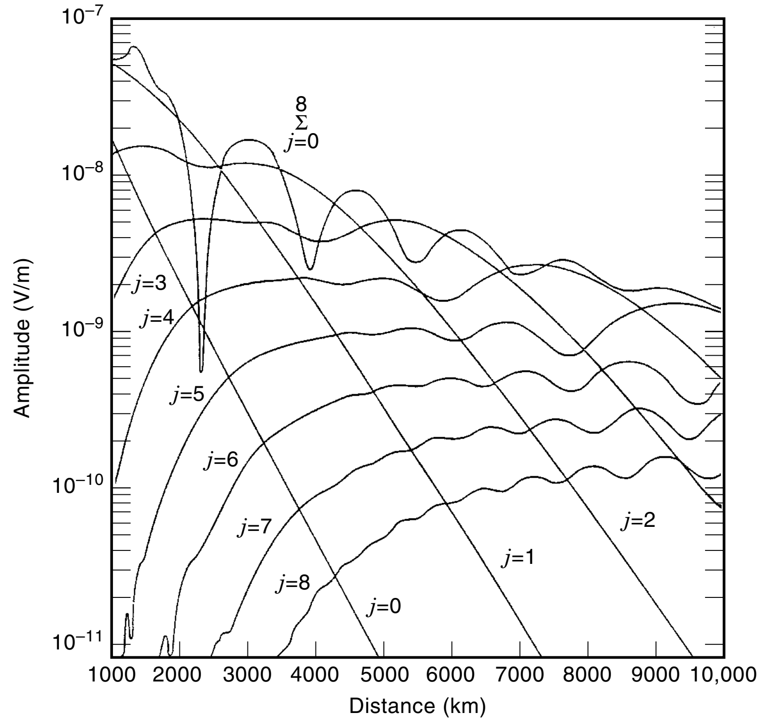

Figure 7. Sample wave hop calculation using the full magneto-ionic theory for the model given in Table 2, for a propagation path over sea water with magnetic parameters and ionosphere electron density profiles given in Ref. 21.

The frequency is 26 kHz, and the ionosphere height $h = 65$ km.

A more sophisticated model of the ionosphere is shown in Fig. 6. Here a single sharply bounded electron plasma slab is placed at 65 km and extends uniformly out to infinity with a constant ratio of electron density to collision frequency of 9.375 (1). The frequency is again 26 kHz. The influence of a finitely conducting ionosphere is here introduced into the model. Again, each sky wave at great distance attenuates with a slope parallel to that of the ground wave on this linear distance–decibel (logarithmic) amplitude scale. A rather interesting set of standing waves as a function of distance appears at shorter distances on the higher-order wave hops. The total field, which sums the wave hops together with the ground wave, does not give any evidence of the existence of these waves.

It is concluded from Fig. 6 that the inclusion of a finitely conducting ionosphere is an important improvement in the modeling technique. At this juncture one could still go further with the full-wave solution and use concentric spherical shells that follow known electron-density–collision-frequency profiles such as given in Ref. 1. But this would not take into account the effects of the earth's magnetic field on the propagation. By following the procedures dictated by Eq. (20) or by using the asymptotic methods used with Eq. (28), the effects of a more realistic model can be generated as shown in Fig. 7. The electron density profile for the ionosphere is given in Ref. 21.

It is interesting to note that the standing waves on the individual wave hops are more highly damped as a function of distance. This is quite reasonable, since the ionosphere lower boundary is more diffuse (gradual) in this model. It therefore seems quite justified to use this more sophisticated model.

BIBLIOGRAPHY

1. J. R. Johler, Spherical wave theory for MF, LF, and VLF propagation, *Radio Sci.,* **5**: 1429–1443, 1970.
2. J. R. Johler, Propagation of the low-frequency radio signal, *Proc. IRE,* **50** (4): 404–427, 1962.
3. J. S. Belrose, L. A. Bound, and L. W. Hewitt, Ground based radio wave propagation studies of the lower ionosphere, *Proc. Conf.,* held 11–15 April 1966, Defence Research Telecommunications Establishment, Radio Physics Lab., Defense Research Board, Dept. of National Defence, Shirley Bay, Ottawa, Canada, 1967.
4. J. R. Johler and L. A. Berry, On the effect of heavy ions on LF propagation, with special reference to a nuclear environment, Natl. Bur. Stand. Tech. Note 313, Washington: U.S. Govt. Printing Office, 1965.
5. D. R. Hartree, *Proc. Cambridge Philos. Soc.,* **25**: 27, 1927.
6. D. R. Hartree, The propagation of electro-magnetic waves in a refracting medium in a magnetic field, *Proc. Cambridge Philos. Soc.,* **27**: 143, 1931.
7. E. V. Appleton, *J. Inst. Elec. Eng.,* **71**: 642, 1932.
8. J. A. Ratcliffe, *The Magneto-ionic Theory and Its Applications to the Ionosphere,* Cambridge, UK: Cambridge Univ. Press, 1959.
9. J. R. Wait, *Electromagnetic Waves in Stratified Media,* New York: Pergamon, 1962.
10. G. Hefley, *The Development of Loran-C Navigation and Timing,* NBS Monograph 129, Washington: U.S. Govt. Printing Office, 1972.
11. J. R. Johler, Propagation of an electromagnetic pulse from a nuclear burst, *IEEE Trans. Antennas Propag.,* **AP-15**: 256–263, 1967.
12. H. Bremmer, *Terrestrial Radio Waves,* New York: Elsevier, 1949.
13. L. A. Berry, Wave hop theory of long distance propagation of LF radio waves, *J. Res. Natl. Bur. Stand.,* **68D**: 1275–1282, 1964.

14. J. R. Johler and J. D. Harper, Jr., Reflection and transmission of radio waves at a continuously stratified plasma with arbitrary magnetic induction, *J. Res. Natl. Bur. Stand.,* **66D**: 81–91, 1962.
15. J. R. Johler and J. D. Harper, Jr., On the effect of a solar disturbance on the LF ionosphere reflection process, *6th AGARD (NATO) Ionospheric Research Meeting,* 15–18 May 1961, Naples, Italy, New York: Pergamon, 1963.
16. J. R. Johler, On radio wave reflections at a continuously stratified plasma with collisions proportional to energy and arbitrary magnetic induction, *Proc. Int. Conf. Ionosphere,* Imperial College, London, July, 1962, London: Inst. Phys., Phys. Soc., Chapman & Hall, 1963.
17. R. M. Davis and L. A. Berry, A revised model of the electron density in the lower ionosphere, Alexandria, VA: Defense Documentation Center, Cameron Station, 1977.
18. M. Abromowitz and I. A. Stegun, *Handbook of Mathematical Functions,* NBS, AMS 55, Washington: U.S. Govt. Printing Office, 1964.
19. L. A. Berry, G. Gonzalez, and J. L. Lloyd, Wave hope series for an anisotropic ionosphere, *Radio Sci.,* **4**: 1021–1027, 1969.
20. J. R. Johler, Zonal harmonics in low frequency terrestrial radio wave propagation, Natl. Bur. Stand. Tech. Note 335, Washington: Supt. of Documents, U.S. Govt. Printing Office, 1966.
21. J. R. Johler and C. Mellecker, Theoretical LF, VLF field calculations with spherical wave functions of integer order, ESSA Tech. Rep. ERL 165ITS 106, Boulder, CO: U.S. Dept. of Commerce, Inst. for Telecommunication Sciences (ITS), 1970.
22. L. A. Berry and J. E. Herman, A wave hop propagation program for an anisotropic ionosphere, OT/ITS Res. Rep. 11, Boulder, CO: U.S. Dept. of Commerce, Inst. for Telecommunication Sciences (ITS), 1971.
23. J. K. Oliver, Jr., G. Gonzalez, and J. L. Lloyd, LF–VLF propagation analysis computer program documentation, RADC-TR-68-453, Rome, NY: Rome Air Development Center, 1968.
24. J. R. Johler and L. A. Berry, *A Complete Mode Sum for LF, VLF, ELF Terrestrial, Radio Wave Fields,* NBS Monograph 78, Washington: U.S. Govt. Printing Office, 1964.
25. J. R. Wait, A diffraction theory for LF sky-wave propagation, *J. Geophys. Res.,* **66**: 1713–1724, 1961.
26. K. Davies, *Ionospheric Radio Propagation,* NBS Monograph 80, Washington: U.S. Govt. Printing Office, 1965.
27. A. V. Phelps, Propagation constants for electromagnetic waves in weakly ionized, dry air, *J. Appl. Phys.,* **21**: 1723–1729, 1960.
28. P. Molmud, Langevin equation and the ac conductivity of non-maxwellian plasmas, *J. Phys. Res.,* **114**: 29–32, 1959.
29. R. B. Dingle, D. Arndt, and S. K. Roy, The integrals $E_p(x)$ and $D_p(x)$ and their tabulation, *Appl. Sci. Res.,* **6B**: 155–164, 1956.
30. L. A. Berry and M. C. Chrisman, Numerical values for the path integrals for low and very low frequencies, NBS Tech. Note 319, Washington: U.S. Govt. Printing Office, 1965.
31. O. E. H. Rydbeck, On the propagation of radio waves, *Trans. Chalmers Univ.* 34, 1944.

Reading List

L. A. Berry and R. M. Jones, A time-varying electron density model for LF/VLF propagation calculations, OT/ITSTM 3, Boulder, CO: U.S. Dept. of Commerce, Inst. for Telecommunication Sciences (ITS), 1970.

J. R. Johler, On the analysis of LF ionospheric radio propagation phenomena, *J. Res. Natl. Bur. Stand Radio Propag.,* **65D**: 5, 1961.

J. R. Johler, Theory of propagation of low frequency terrestrial radio waves—mathematical techniques for the interpretation of D-region propagation studies, *1966 Ottawa Conf. Proc.,* Vol. 2, 1967, pp. 399–422. See also Ref. 3.

J. R. Wait, Terrestrial propagation of very low frequency radio waves, *J. Res. Natl. Bur. Stand. D Radio Propag.,* **64D**: 183–204, 1960.

J. RALPH JOHLER
Johler Associates